Characterization of the Morphological Changes in Linear Low-Density Polyethylene during the Melting Process Using Synchrotron Radiation

P. Schouterden, M. Vandermarliere, C. Riekel,† M. H. J. Koch,‡ G. Groeninckx, and H. Reynaers*

Laboratory of Macromolecular Structural Chemistry, Katholieke Universiteit Leuven, Celestijnenlaan 200 F, B-3030 Leuven, Belgium, and Institut für Technische und Makromolekulare Chemie, University of Hamburg, Bundesstrasse 45, D-2000 Hamburg 13, West Germany. *Received January 20, 1988; Revised Manuscript Received May 31, 1988*

ABSTRACT: Time-resolved SAXS diffraction data—as obtained by synchrotron radiation—of isothermally crystallized linear low-density polyethylenes with propene and 1-octene as the comonomer have been used to clarify the complex morphology of these samples. The data have been obtained under DSC conditions where, for most of the samples, up to four melting endotherms can be detected. On the basis of long spacing and invariant analysis, combined with fractionation experiments, it can be shown that the morphology involves phase segregation and results from sample heterogeneity both with respect to molecular weight and comonomer distribution, type, and content; these parameters affect crystal thickness, crystal perfection, crystallinity, and melting behavior. The melting domain of all samples starts as low as ±38 °C and extends up to final melting at ±130 °C. The classical two-phase model cannot be used to quantify all the observed data.

Introduction

Linear low-density polyethylenes (LLDPE's) are heterogeneous copolymers of ethylene and an α-olefin (like propene, 1-butene, 1-hexene, or 1-octene). In the bulk state, these materials have a semicrystalline spherulitic morphology, composed of alternating crystalline lamellae and amorphous regions. The comonomer units are present as short side branches on the main chain; their type, amount, and distribution along the main chain will affect the thickness and perfection of the crystalline lamellae, the sample crystallinity, and the melting behavior.

The melting curve of isothermally crystallized LLDPE's, studied with a differential scanning calorimeter (DSC),[1] exhibits several melting endotherms (two, three, or four), depending on the crystallization temperature and the comonomer type, content, and distribution. This complex melting behavior indicates a broad distribution of the thickness and perfection of the lamellar crystals. Fractionation experiments[2] reveal that this morphology is the result of a molecular heterogeneity, with respect to both the molecular weight and the comonomer distribution.

The melting of LLDPE copolymers occurs, in general, between 40 and 130 °C. With a typical DSC heating rate of 5 °C/min, the determination of a melting profile takes about 20 min. In order to understand the very complex morphology of these materials, it is of interest to examine the behavior of some important morphological parameters such as the mean long spacing and the invariant during the melting process. Using a conventional X-ray generator in the laboratory, the recording of one SAXS pattern, representative for the morphology at a given temperature, requires much more time than the total melting process. As a consequence, this approach is not appropriate for the characterization of morphological changes during the melting process. Using a synchrotron X-ray source, however, it is possible to record a complete SAXS pattern in every 2 °C interval of the melting process, thus allowing the evolution of the morphology to be followed. The potential use of synchrotron radiation in conjunction with DSC has been demonstrated recently in other reports[1,3,4] and Grubb et al.[5-7] have followed the annealing of polyethylene single-crystal mats using dynamic SAXS at a synchrotron source.

In this research time-resolved SAXS patterns of propene and 1-octene LLDPE's have been recorded under melting conditions, identical with those during DSC experiments. As a basis for the discussion of the more complex LLDPE data, DSC and synchrotron radiation scattering experiments on HDPE were performed initially. All experiments on the different materials were performed under the same conditions. In order to allow a detailed comparison of both methods, the DSC traces for each specimen are presented first, followed by the SAXS data.

Table I
Molecular Characteristics and Crystallinity of the HDPE and LLDPE Specimens

PE type	code	M_w[a]	M_w/M_n[b]	av CH_3/1000 C	X_c,[c]
HDPE	H1	83 000	3.4	0.0	77
propene LLDPE	P1	91 000	7.1	4.2	65
	P2	63 500	7.2	17.7	39
	P3	94 000	8.6	28.4	22
1-octene LLDPE	O1	119 000	4.1	6.8	51
	O2	119 000	4.0	10.3	38
	O3	93 000	4.0	14.0	35

[a] Weight-average molecular weight. [b] Polydispersity index. [c] DSC crystallinity.

Experimental Section

Materials. The following samples were studied: (1) a linear polyethylene (HDPE) sample used as reference (H1); (2) three ethylene/propene copolymers with a different average propene content (P1, P2, and P3); (3) three ethylene/1-octene copolymers with a different average 1-octene content (O1, O2, and O3).

All samples were isothermally crystallized from the melt under a nitrogen atmosphere at T_c = 105 °C for 17 h and subsequently cooled slowly to room temperature. The molecular characteristics are listed in Table I.

DSC Measurements. For the differential scanning calorimetry measurements, a Perkin-Elmer DSC-2C was used. The heating rate was 5 °C/min. The crystallinity of the HDPE and LLDPE samples was calculated by integration of the DSC signal. As reference for a 100% crystalline PE, ΔH = 293 J/g was taken.[8]

Determination of the Comonomer Concentration. The average degree of short-chain branching of the LLDPE specimens was determined by ^{13}C NMR spectroscopy (NMR Bruker WM250 Cryospec, PW = 60°, PD = 10 s), according to the ^{13}C chemical shifts for ethylene/α-olefins established by Randall.[9] Fraction-

† University of Hamburg. Present address: European Synchrotron Radiation Facility, F-38043 Grenoble Cedex, France.
‡ EMBL c/o DESY, Notkestr. 85, D-2000 Hamburg 52, W. Germany.
* To whom correspondence should be addressed.

0024-9297/89/2222-0237$01.50/0

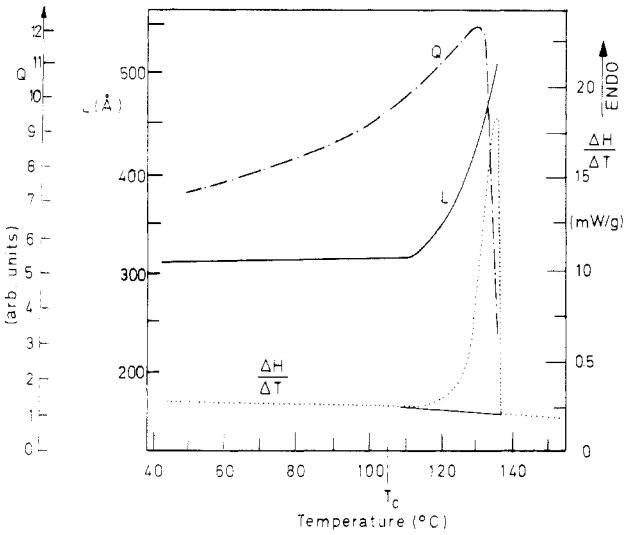

Figure 1. DSC melting curve and evolution of the long spacing L and of the invariant Q for isothermally crystallized (T_c = 105 °C) linear polyethylene HDPE (specimen H1).

ation experiments with respect to the comonomer distribution using the analytical temperature rising elution fractionation (ATREF) method indicate a very wide intermolecular distribution of the short-chain branches.[2]

Determination of the Molecular Weight and Molecular Weight Distribution. The average molecular weight and the molecular weight distribution of the different samples were determined by using high-temperature gel permeation chromatography at 140 °C with 1,2,4-trichlorobenzene as solvent (Waters GPC).

Determination of the Unit Cell Parameters Using Wide-Angle X-ray Scattering (WAXS). WAXS patterns were recorded at room temperature and at T_c in the reflection mode with a Philips vertical diffractometer equipped with a proportional counter and a pulse-height analyzer. Ni-filtered Cu Kα radiation with a wavelength of 1.542 Å was used. The a and b unit cell parameters were calculated from the (200) and (110) reflections. The c parameter was constant and equal to 2.547 Å.

Synchrotron Radiation Experiments. All dynamic synchrotron radiation experiments were performed at the polymer beam line of HASYLAB-DESY (Deutsches Electronen Synchrotron), which is located at the storage ring DORIS[10-12] in Hamburg. The double-focusing camera was operating at a wavelength of 1.5 Å. The sample-to-detector distance was about 2.5 m. DORIS was operating in a dedicated mode at 3.7 GeV, with a maximum current of 80 mA and about 2 h lifetime of the beam. A programmable furnace[10] was used to heat the samples from 40 to 150 °C at a heating rate of 5 °C/min. SAXS spectra were recorded every 2 °C with a one-dimensional position-sensitive detector, which corresponds to a counting time of 24 s per pattern. The patterns were calibrated by a piece of dry bovine cornea. The long spacing L was calculated by applying Bragg's law to the SAXS peak maximum. The invariant Q is the total scattering power of the speciment and can be calculated for pinhole-collimation conditions by

$$Q = \int_0^\infty s^2 I(s)\, ds \qquad (1)$$

with $s = 2 \sin \theta/\lambda$, 2θ = scattering angle, and $I(s)$ = scattered intensity. All patterns were corrected for background scattering by subtracting the scattering of a blank sample holder, Lorentz-corrected, and smoothed by using cubic splines.

Experimental Results and Discussion

Linear Polyethylene HDPE (Specimen H1). The DSC trace of the HDPE specimen, recorded at a heating rate of 5 °C/min, is shown in Figure 1. A single melting endotherm with a maximum at 135 °C is observed; the first indication of melting occurs at 110 °C. Figure 2 shows a pseudo-3D plot of the time-resolved SAXS patterns recorded under the same conditions. The second-order peak remains present close to final melting, an indication of a well-ordered morphology.

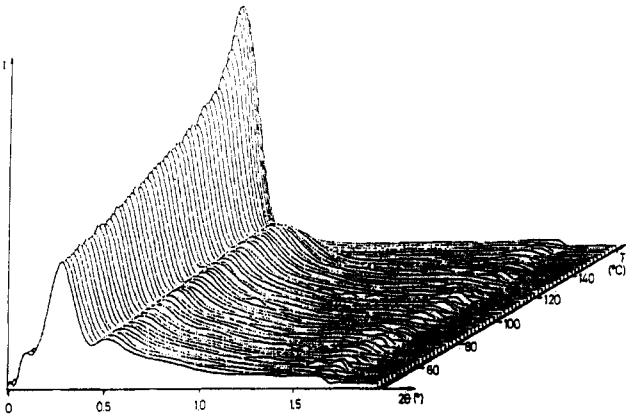

Figure 2. Time-resolved SAXS spectra of HDPE (specimen H1), recorded during linear heating.

The evolution of the invariant Q and the long spacing L is shown in Figure 1, superimposed on the DSC trace. The long spacing L remains almost unchanged up to 110 °C, where melting is first observed in the DSC. The small increase of L (±15 Å), observed between room temperature and T_c, is due to the thermal expansion of the amorphous phase which separates the crystalline layers. The discontinuity in long spacing coincides with the onset of the endothermic peak in the DSC trace. The strong increase in long spacing L is caused by the continuous melting of the less stable crystalline lamellae in the stacks. Due to the limited resolution of the camera and the lack of information with respect to the volume fraction of the spherulites at the ultimate stages of melting, it was not possible to obtain reliable data for L and Q up to complete melting.

The continuous increase of the invariant Q between room temperature and the onset of melting can be explained in terms of the different expansion coefficients of the crystalline (α_c) and amorphous (α_a) phases, as shown by Fischer:[13]

$$\left(\frac{Q(T)}{Q(T_0)}\right)^{1/2} = 1 + \frac{(\alpha_a - \alpha_c)(T - T_0)}{|\Delta\rho_0|} \qquad (2)$$

$Q(T_0)$ is the invariant at a given reference temperature, $\Delta\rho_0$ stands for the electron density difference between the crystalline and amorphous layers at temperature T_0, and α_c and α_a are the thermal expansion coefficients of the crystalline and amorphous phases, respectively. For these thermal expansion coefficients, the following values were used:[14] $\alpha_c = 8.024 \times 10^{-4}$ K^{-1} and 8.78×10^{-4} K$^{-1} < \alpha_a < 11.24 \times 10^{-4}$ K^{-1}.

In Figure 3, the calculated and measured values for $Q(T)/Q(T_0)$ are plotted for the temperature range 40–110 °C. The experimental curve fits best to the upper limit value reported for α_a.

In the melting region, the invariant Q can be correlated with the instantaneous crystallinity X_c and the electron density difference, $\Delta\rho = \rho_c - \rho_a$, between the crystalline and amorphous regions:

$$Q = K\langle\Delta\rho^2\rangle \qquad (3)$$

In this relation, K stands for a number of constant factors involving apparatus conditions and the scattering of a free electron, and $\langle\Delta\rho^2\rangle$ is the mean square of the electron density fluctuations:

$$\langle\Delta\rho^2\rangle = X_c(1 - X_c)(\rho_c - \rho_a)^2 \qquad (4)$$

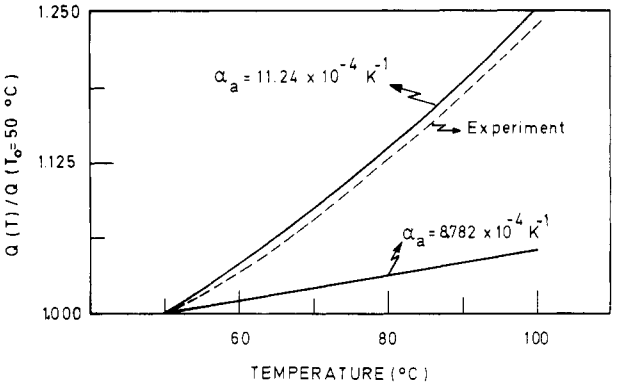

Figure 3. $Q(T)/Q(T_0)$ as a function of temperature for linear polyethylene (specimen H1), compared with literature values reported for α_a.

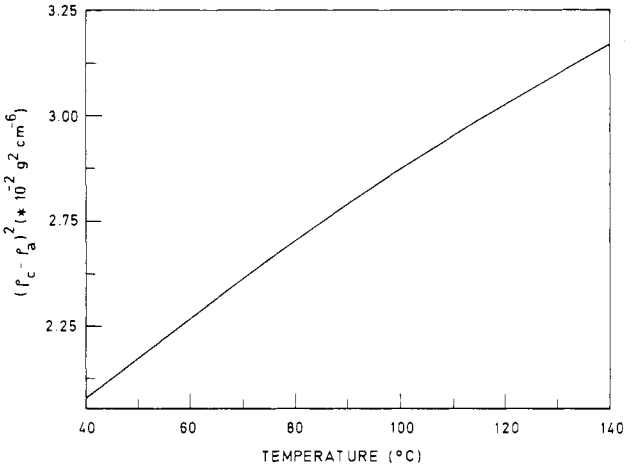

Figure 4. Dependence of the square of the density difference on the temperature.

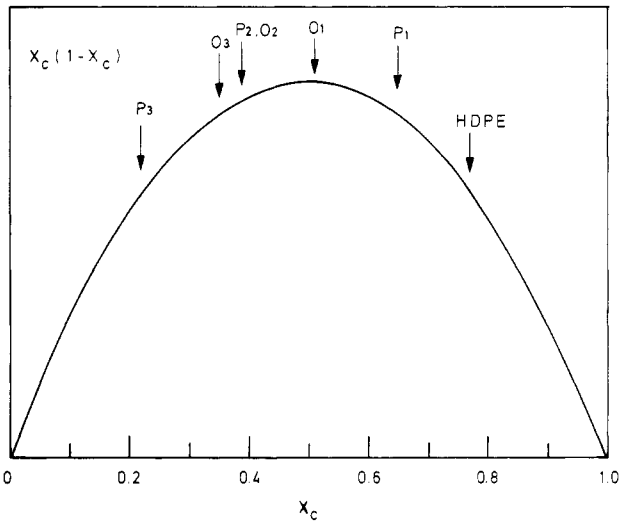

Figure 5. The term $X_c(1 - X_c)$ as a function of the crystallinity X_c. The degree of crystallinity at room temperature for the samples is indicated.

where X_c = volume crystallinity of the sample. For measurements on a relative scale, K can be eliminated from eq 3. The temperature dependence of the physical densities η of the crystalline and amorphous zones is obtained from the formulas of Swan:[15]

$$\eta_c^{-1} = 0.994 + 2.614 \times 10^{-4}T + 4.43 \times 10^{-7}T^2 \quad (5)$$

$$\eta_a^{-1} = 1.152 + 8.8 \times 10^{-4}T \quad (6)$$

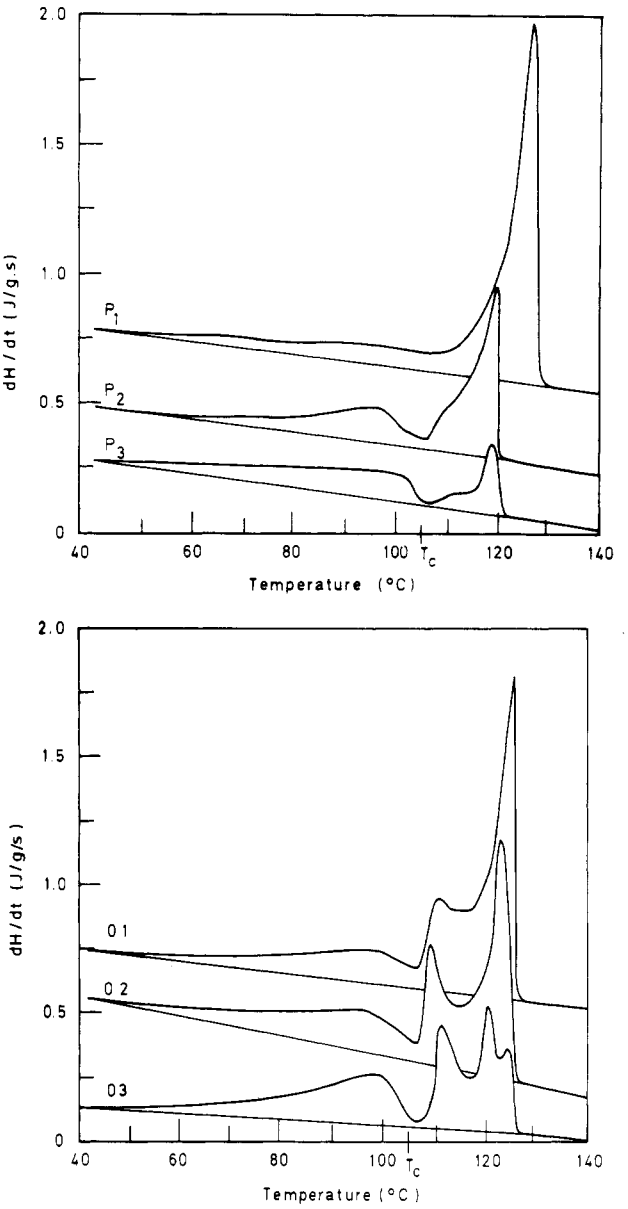

Figure 6. DSC melting curves of isothermally crystallized (T_c = 105 °C) propene (a, top) and 1-octene (b, bottom) LLDPE's.

where T is the temperature expressed in °C and η_c^{-1} and η_a^{-1} are reciprocal mass densities (cm^3/g) to be transformed to electron densities.

The term $(\rho_c - \rho_a)^2$ is an increasing function with temperature (see Figure 4), while $X_c(1 - X_c)$ is a parabolic function with its maximum value at $X_c = 0.50$ (see Figure 5).

The behavior of the invariant above 110 °C (the temperature where the long spacing starts to increase as a consequence of melting) is due to the combined change in the electron density contrast $(\rho_c - \rho_a)$ and the decrease of crystallinity X_c (eq 4). Due to the high crystallinity of the HDPE specimen at room temperature ($X_c = 0.77$), a decrease in X_c will initially increase the factor $X_c(1 - X_c)$ until $X_c = 0.50$ is reached (see Figure 5). These two factors explain therefore why an increase in Q is observed up until 132 °C. At 132 °C, the increasing $(\rho_c - \rho_a)$ and the decreasing X_c are competitive. The influence of the crystallinity decrease on Q, as a result of melting, becomes obviously dominating above 132 °C.

LLDPE Copolymers. The DSC traces of the LLDPE samples investigated are shown in Figure 6. These traces can be divided empirically into three regions.

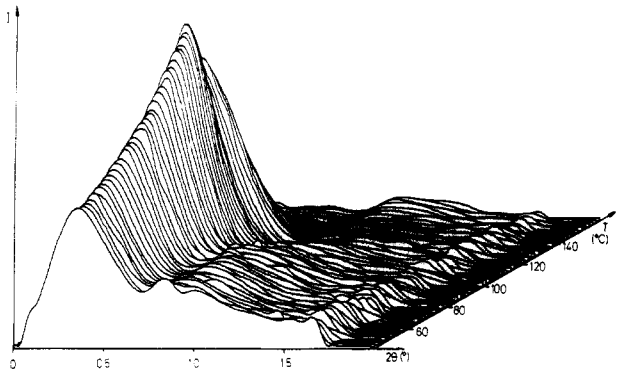

Figure 7. Time-resolved SAXS spectra of a 1-octene LLDPE (specimen O2), recorded during linear heating.

Region 1. This region extends to the isothermal crystallization temperature T_c = 105 °C. In this temperature range, the crystals, which must have been formed as a segregated phase below T_c, melt.[1]

Region 2. This is the most complex part of the DSC trace. Depending on the molecular characteristics of the sample and the crystallization temperature, one or two melting endotherms are observed. These endotherms represent the melting of the crystals which were formed at the isothermal crystallization temperature.

Region 3. The single endotherm corresponding to region 3 is ascribed to the melting of crystals formed at T_c and originates from molecular segments with very few or no comonomeric side branches. This conclusion is derived on the basis of recent fractionation experiments.[2]

Several problems occur in the evaluation of the DSC curves. The onset of first melting cannot be determined exactly, as a consequence of uncertainties in the background of the DSC heat flux. Further, peak overlaps make it difficult to resolve the complex melting processes occurring in region 2. The onset of melting was determined by independent WAXS measurements during linear heating from room temperature by continuous monitoring of the (110) reflection in the oscillation mode: the intensity of the (110) reflection starts to decrease at 39–40 °C for all LLDPE samples, due to a decrease of crystallinity (melting of crystals). This broad melting range is an indication of a very heterogeneous morphology, caused by a heterogeneity on a molecular level (regarding the molecular weight distribution as well as the comonomer distribution).[2]

Figure 7 shows the evolution of the SAXS spectrum for 1-octene LLDPE (sample O2), which is representative for all other LLDPE samples. The evolution of the invariants is shown in parts a and b of Figure 8, for the 1-octene and propene samples, respectively. The evolution of the long spacing is plotted in Figure 9.

The SAXS patterns of the LLDPE's differ from the HDPE patterns by the width of the peak, which suggests a broader distribution of crystalline lamellae. Furthermore, a second-order peak is not observed. As the temperature is raised, the height of the scattering maximum increases and its position shifts toward lower 2θ values (or larger long spacings).

A more detailed analysis of the parameters, plotted in Figure 9, shows further differences.

The observed behavior of the long spacing can be understood with respect to the DSC behavior. The first broad melting endotherm in the DSC trace (region 1) has been ascribed to the melting of thin and imperfect crystalline lamellae, which were formed below the isothermal crystallization temperature T_c = 105 °C.[1] From electron microscopy observations[16] it appears that these lamellae

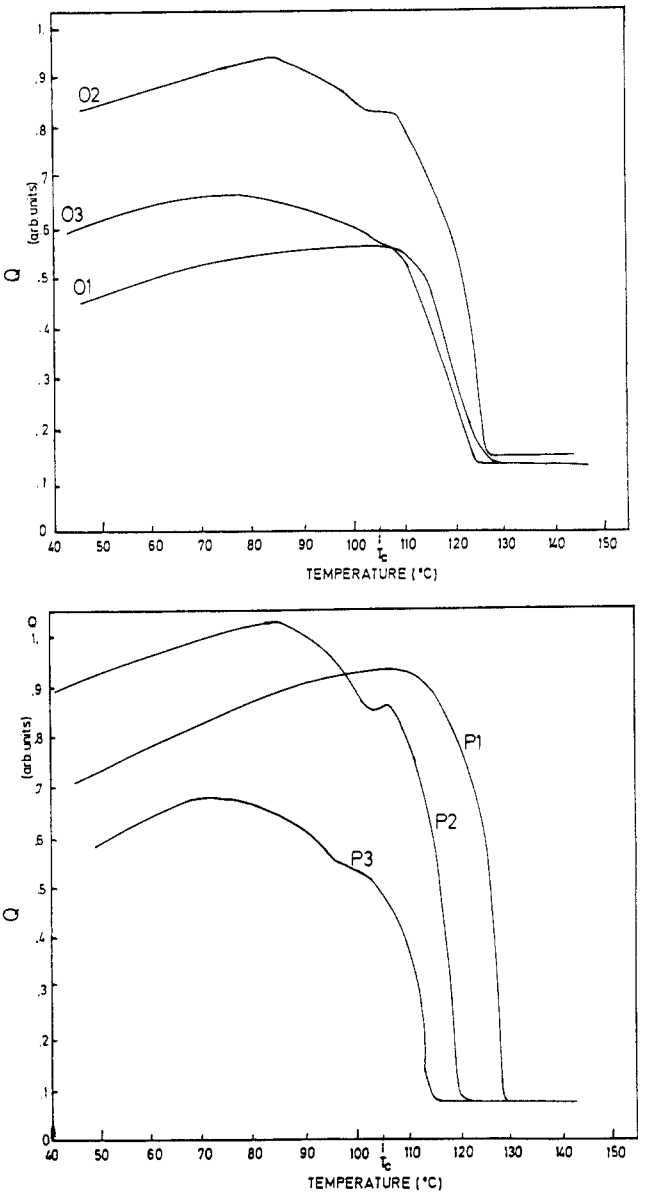

Figure 8. Evolution of the invariant Q (arbitrary units) as a function of the temperature for 1-octene (a, top) and propene (b, bottom) LLDPE copolymers.

Table II
Relative Increase of the Long Spacing $\Delta L/L$ as a Function of the Average Branch Content for LLDPE Samples

code	av CH_3/1000 C	$\Delta L/L$, %	code	av CH_3/1000 C	$\Delta L/L$, %
O1	6.8	36	P1	4.2	26
O2	10.3	83	P2	17.7	119
O3	14.0	188	P3	28.4	178

are located between the ones formed at T_c. They melt preferentially on heating in the DSC, causing an increase of the long spacing L. Above 105 °C, it becomes more difficult to observe a distinct SAXS peak maximum, due to strong scattering close to the primary beam. The relative change in long spacing $\Delta L/L$ increases with comonomer content, because specimens with a higher branching content contain a higher amount of crystalline segregated phase (region 1) (see Table II). The distinction between regions 1, 2, and 3 in the DSC trace is not observed in the evolution of the SAXS parameters; there is no sudden increase in their slopes, which could be associated with the onset of one of the melting endotherms.

Although the present results only refer to LLDPE samples of complex molecular composition, some of the data

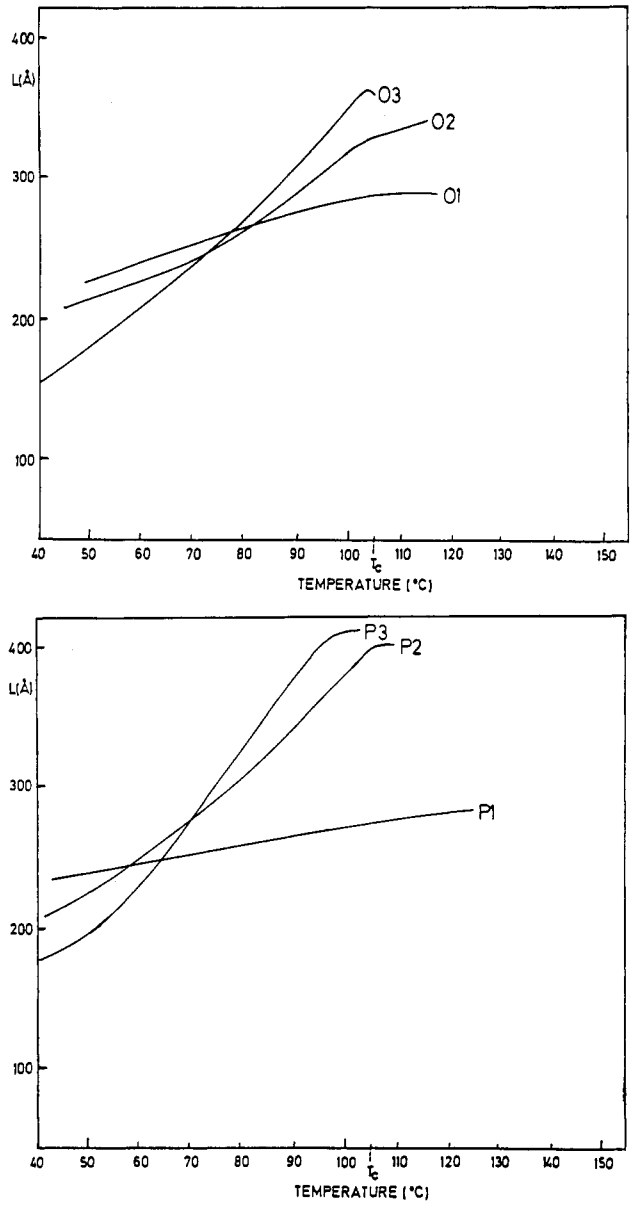

Figure 9. Evolution of the long spacing L as a function of the temperature for 1-octene (a, top) and propene (b, bottom) LLDPE copolymers.

exhibit similarities with observations made by other authors. Strong changes in long spacing on melting have been reported for LDPE by Strobl et al.[17] According to these authors the essential factor governing melting and crystallization behavior of the samples is the thickness distribution in the amorphous layers; in agreement with our own conclusions it was found that lamellae formed at lower temperatures are thinner and include more defects.

In order to give full account of the observed changes in long spacing, one is forced to recur to some melting mechanism. According to Fischer et al.,[18] changes in long spacing reflect either partial melting and/or full strand melting of crystallites. Schultz et al.[19] propose criteria to differentiate both phenomena, the former process being characterized by an increase in the intensity of the SAXS curves with no gross overall changes in shape, the latter process—full strand melting—involving the increasing presence of a zero-angle peak. From our data it is not possible to differentiate the two alternatives. Already in region I of the melting process, and for al our LLDPE samples, an increase in both long spacing and scattering power are observed simultaneously. With respect to regions II and III the relevant SAXS information is close to the primary beam and difficult to resolve within the experimental context at the beam line.

Another possible interpretation of our data is offered by some observations of Keller and al.[20,21] on samples of HDPE's and blends of linear and branched polyethylene. In both works there is clear experimental evidence for molecular segregation during crystallization; double lamellar populations either were made directly visible by electron microscopy or became apparent from low-frequency Raman spectroscpy analysis. In agreement with our own results the population of the thinnest, thermally less stable lamellae was ascribed to originate from molecular segregation during crystallization. Indications for this interpretation follow from a number of our own, as yet unpublished, data.[24] It is clear from small-angle light-scattering experiments that on crystallization at T_c, the spherulites are volume-filling. In view of the large amount of segregated material crystallizing below T_c, the new crystals have to accommodate themselves in the space availabe within the existing spherulites, possibly within "pockets". TEM photographs have been obtained on our samples by the Kanig method. However, we failed to detect pocketlike structures as reported by Norton et al.[20] Our own experiments, however, are probably not conclusive for the absence of pocketlike structures, as the staining technique used is rather aggressive. Norton et al.[20] obtained their results on intentionally prepared blends, using materials which are by nature incompatible. If the model of phase segregation involving pockets with a homogeneous defect concentration applies, one would expect a stepwise change of the unit cell volume on heating the sample. In practice, by monitoring the change in cell parameters on melting, one observes a continuous decrease of the cell volume, approaching, close to final melting, the cell volume of HDPE.[16] This again evidences the melting out of the less stable crystals occluded within the frame of thermally more stable lamellae and/or lamellar bundles.

In any case the "long spacing" L is obtained from a broad diffraction peak, which indicates a very wide distribution of L. Therefore, the long spacing in this case should not be interpreted strictly as the mean long spacing of regularly alternating crystalline and amorphous regions in the ideal two-phase concept. This conclusion is supported by inspection of the experimental one-dimensional correlation functions obtained from our data.[16,22,23] These correlation functions appear to be rather diffuse: some exhibit a faint maximum, while in the others no maximum at all can be detected. Moreover, no well-defined horizontal plateau can be found at the first minimum in the correlation function. Consequently the adequacy of a Lorentz correction, as applied to all of our diffraction data, can be questioned. However, it is felt by the authors that the omission of the correction would not affect the trends observed in the present results.

Together with the increase in long spacing, the invariant Q first increases with increasing temperature and decreases dramatically as soon as the crystallization temperature T_c = 105 °C is reached. Interestingly, a slight decrease is observed for samples O3 at about 75 °C and O2 at about 85 °C. A similar observation is also made for samples P2 and P3. Therefore, a more elaborate analysis of the invariant seems appropriate. The observed behavior can be explained qualitatively by again considering eq 4. The first onset of decrease in Q (samples O2, O3, P2, and P3) is due to a dominating influence of the crystallinity decrease. Above T_c, one observes, as expected from the ongoing melting process, a dramtic decrease of Q for all LLDPE samples. The shape of the invariant curves can be simu-

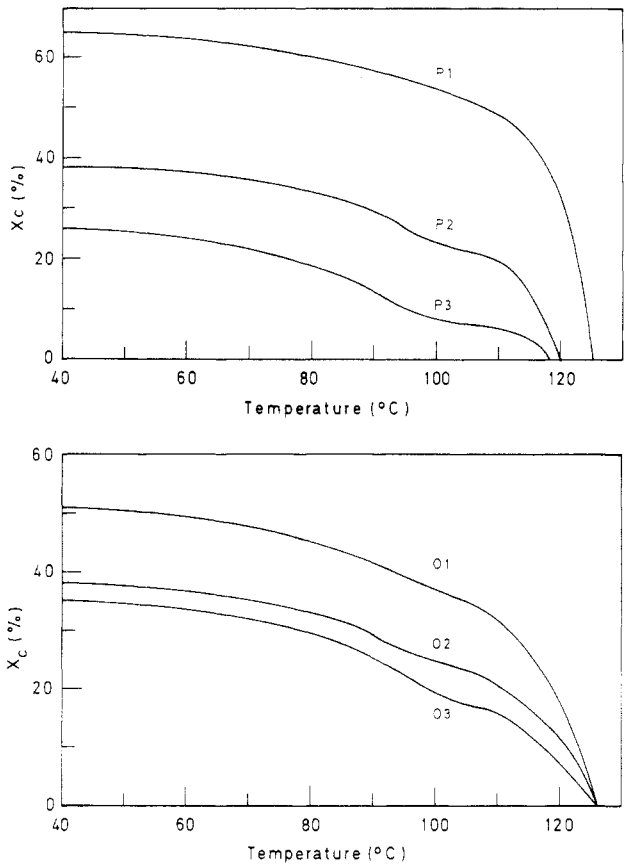

Figure 10. Dependence of the total crystallinity X_c as a function of the temperature (as determined from DSC data) for propene (a, top) and 1-octene (b, bottom) copolymers.

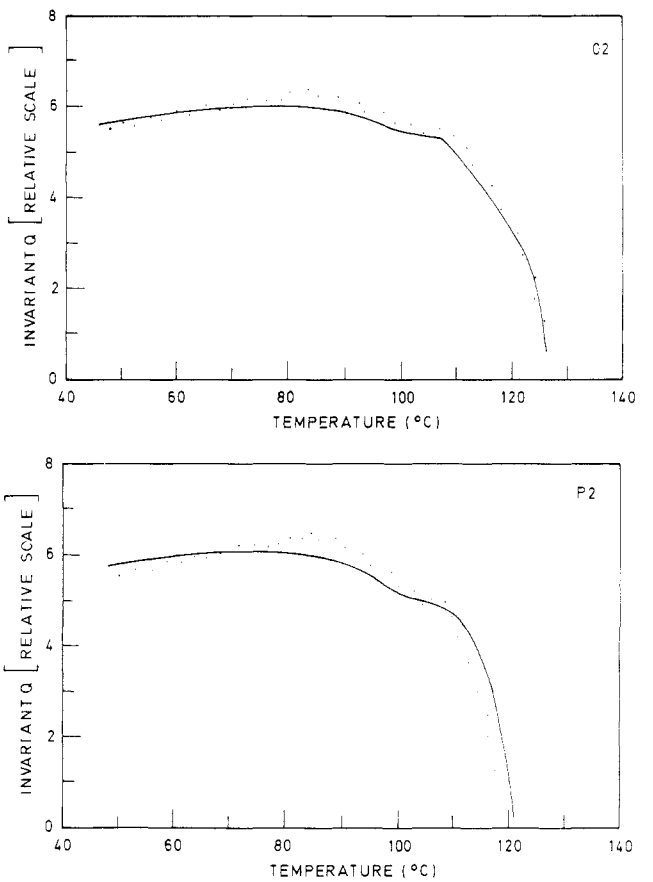

Figure 11. Comparison, after scaling, between the calculated evolution of the invariant and the experimental data for specimen O2 (a, top) and P2 (b, bottom).

lated by calculating a theoretical curve from eq 4 with the instantaneous values for X_c calculated from the DSC thermogram by integration of the partial areas of the DSC heat flux (see Figure 10), and from eq 5 and 6 for $(\rho_c - \rho_a)$. It should be clear that this is only an approximation, because the evolution of the electron density difference is considered only to be dependent on the temperature, while the dependence on the composition of the crystals is neglected. The calculated curves are satisfactorily congruent to the corresponding experimental curves. They are plotted in parts a and b of Figure 11 for specimen O2 and P2 after parallel shifting on the relative scale in order to inspect the coincidence.

More information can be obtained by a combined analysis of DSC traces and the invariant. In order to separate the contribution of the electron density difference $(\rho_c - \rho_a)$ and the crystallinity X_c to the invariant, the evolution of $(\rho_c - \rho_a)$ as a function of temperature was determined by division of the Q curve by the $X_c(1 - X_c)$ curve. Since changes of Q are measured on a relative scale, these values represent relative increases of $(\rho_c - \rho_a)$ rather than absolute values. Above 110 °C, the evaluation of $(\rho_c - \rho_a)$ is inaccurate. The evolution of $(\rho_c - \rho_a)$ is determined by two physical factors: a different temperature dependence of the crystalline and amorphous densities (which is an increasing function with temperature; see eq 5 and 6) and a different composition (and thus a different density) of the crystals formed at different temperatures. Therefore, the $Q/(X_c(1 - X_c))$ values as a function of temperature were corrected for the temperature dependence of $(\rho_c - \rho_a)$, as calculated from eq 5 and 6. The resulting curves for the propene samples are plotted in Figure 12 and represent the relative increase in electron density difference merely due to the changing composition

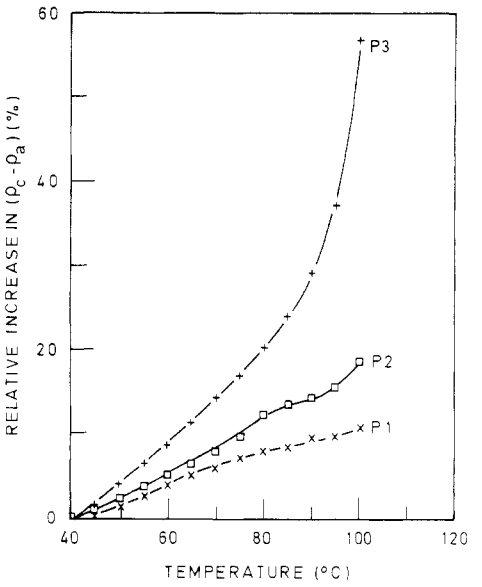

Figure 12. Relative increase of the electron density difference $(\rho_c - \rho_a)$ as a function of the temperature for propene LLDPE's, corrected for thermal expansion.

of the crystals and of the amorphous regions, present at a certain temperature during the DSC scan. As can be seen from Figure 12, all specimens show an increasing $(\rho_c - \rho_a)$ with temperature.

As the density of the amorphous zones ρ_a is constant throughout the composition range, an increase of the crystalline density ρ_c is observed during the melting of the crystallized segregated phase (region 1). This means that crystals, formed at lower temperatures, are more defective than crystals formed at higher temperatures, probably as

Table III
Unit Cell Volume at Room Temperature and at T_c = 105 °C

code	av CH_3/1000 C	unit cell vol at RT, Å^3	unit cell vol at T_c = 105 °C, Å^3	corrected unit cell vol at T_c = 105 °C, Å^3
H1	0.0	94.10	96.82	94.10
O3	14.0	96.25	97.60	94.86
P2	17.7	96.43	97.76	95.01

a result of some incorporation of side-chain branches in the crystals. Similar observations are obtained for the 1-octene samples which are not reported here. Evaluation of the invariant during melting of the spherulites involves the determination of the instantaneous values of the volume fraction of spherulites present at each temperature; because this information is not experimentally available and since the separation of scattering due to the two-phase system becomes increasingly difficult as one approaches total melting, values of $\rho_c - \rho_a$ above T_c are not reported. A the moment there is a clear need for experimental data on an absolute scale to quantify these results.

Independent measurements of the unit cell parameters at room temperature and at 105 °C using wide-angle X-ray measurements (WAXS) are reported in Table III.

The unit cell volume of the LLDPE specimens is larger than the HDPE unit cell volume, probably due to some incorporation of the side branches in the crystals. Furthermore, if the unit cell parameters are measured at T_c = 105 °C, i.e., the temperature where the segregated phase is molten, an increase in cell volume is observed. If one corrects the high-temperature values for thermal expansion on the basis of the expansion of the HDPE sample (which has no crystalline segregated phase), unit cell volumes smaller than those at room temperature are obtained. A more complete study of changes in unit cell volume during heating of our samples will be the subject of a forthcoming paper.[24] The present result (Table III) supports our model that crystals present at T_c are less disturbed, as compared to all the crystals present at room temperature. Fractionation experiments[2] showed that the strongly defected crystals of the segregated phase are composed of molecules that are richer in side branches. These more defective crystals melt at lower temperatures, thus leaving the more perfect crystals, which consequently have a higher electron density and a smaller unit cell volume. Other authors[25-27] have also observed an expansion of the unit cel of ethylene copolymers due to the incorporation of short side branches. However, both methods determine an average value over all the crystals and over possibly heterogeneous crystals. Therefore, our results give no definite answer whether or not the crystal imperfection has to be attributed to comonomeric side branches located at the surface of the crystals or to side branches accommodated in the core of the crystals. Very recently,[28] a study using nitric acid oxidation and solvent extraction techniques pointed out that the majority of ethyl, butyl, and hexyl branches are excluded from the core of the crystals. A high-resolution solid-state ^{13}C NMR study[29] led to the conclusion that a small amount of methyl short chain branches (propene LLDPE) can be accommodated in the core of the crystals; longer branches (1-butene, 1-hexene, and 1-octene LLDPE) in the crystal cores can hardly be detected within the limits of instrumental sensitivity.

Conclusions

Time-resolved SAXS diffraction data of isothermally crystallized propene and 1-octene LLDPE's and a HDPE specimen have been recorded during the melting process by using synchrotron radiation. The experimental conditions were the same as during the dynamic scanning calorimetry (DSC) experiments.

For all LLDPE samples, the mean long spacing increases smoothly without sudden changes at the onset of one of the melting endotherms. These experimental observations reflect a broad distribution of the structural long spacing in the LLDPE specimens.

The relative change in long spacing $\Delta L/L$ during the melting process is dependent on the average comonomer content, with more pronounced changes at higher contents. The distribution of the lamellar spacing is broader for higher branch contents. As a consequence of molecular heterogeneity and limited resolution at the beam line the present results give no clear-cut answer as to the melting mechanism(s) involved.

The electron density difference ($\rho_c - \rho_a$), calculated from both the experimental invariant and crystallinity data, increases with temperature. This results from the melting of the less perfect (more defect) crystals of the crystalline segregated phase, which is formed at temperatures below T_c.

A more pronounced incorporation of side branches in the crystals is observed for propene LLDPE than for 1-octene LLDPE. The incorporation of the comonomeric side branches in the crystals is supported by preliminary measurements of the unit cell volume at room temperature and at the crystallization temperature T_c = 105 °C. However, on the basis of the present results, no definite conclusion can be made about the location of side groups in the crystals (at the surface or in the core).

The present results make it clear that the semicrystalline morphology of LLDPE copolymers cannot be described adequately with the ideal two-phase model.

In the case of the HDPE specimen, which has no crystallized segregated phase, the long spacing remains almost constant between 40 °C and the onset of melting (110 °C). The slight increase in the long spacing is due to the thermal expansion of the specimen during the linear heating process. Above 105 °C, there is a sharp increase in long spacing, caused by the selective melting of the less stable crystals in the lamellar stacks. The invariant Q increases continuously before dropping steeply in the vicinity of the final melting temperature. Clearly, the HDPE specimen has a much more narrow distribution of the distances between crystalline lamellae and a more uniform distribution of the crystal thicknesses, consequently HDPE is closer to the ideal two-phase model than LLDPE.

Further experimental progress might be expected from careful WAXS experiments to monitor the unit cell parameters upon heating, as the different melting endotherms present might imply crystals involving small changes in unit cell parameters. Also, unit cell measurements and SAXS experiments on fractionated LLDPE's will be of great interest.

Furthermore, SAXS experiments would have to be extended to lower diffraction angles in order to determine the change of the SAXS parameters (long spacing, crystal thickness, and invariant) above T_c = 105 °C as well as to decide on the mechanism and models involved to explain the strong changes in long spacing.

In any case, dynamic diffraction experiments using synchrotron radiation have been shown to be a promising powerful tool for the understanding of a complex melting behavior as observed in the DSC.

Acknowledgment. We thank the Dow Chemical Co. (Terneuzen, Netherlands) for financial support given to the laboratory; we are also indebted to Dr. F. Jansen and Ir. B. Van der Heijden (Olefin Plastics Research) for in-

teresting discussions and their excellent contribution in the fractionation experiments. C. Riekel and H. Reynaers are indebted to HASYLAB, to NATO for a Collaborative Research Grant (85/0612), and to NFWO and FKFO of Belgium for research and travel grants.

Registry No. (Ethylene)(propene) (copolymer), 9010-79-1; (ethylene)(1-octene) (copolymer), 26221-73-8.

References and Notes

(1) Schouterden, P.; Groenickx, G.; Reynaers, H.; Riekel, C.; Koch, M. H. J. *Polym. Bull. (Berlin)* **1985**, *13*, 533.
(2) Schouterden, P.; Groeninckx, G.; Van der Heijden, B.; Jansen, F. *Polymer* **1987**, *28*, 2099.
(3) Russell, T. R.; Koberstein, J. T. *J. Polym. Sci., Polym. Phys. Ed.* **1985**, *23*, 1109.
(4) Song, H. H.; Stein, R. S.; Wu, D.-Q.; Ree, M.; Phillips, J. C.; LeGrand, A.; Chu, B. *Macromolecules* **1988**, *21*, 1180.
(5) Grubb, D. T. *Polym. Prepr. (Am. Chem. Soc., Div. Polym. Chem.)* **1983**, *24*, 296.
(6) Grubb, D. T.; Liu, J. J. H.; Caffrey, M. *J. Polym. Sci., Polym. Phys. Ed.* **1984**, *22*, 567.
(7) Grubb, D. T.; Liu, J. J. H. *J. Appl. Phys.* **1985**, *58*, 2822.
(8) Wunderlich, B. *Macromolecular Physics*; Academic Press: New York, 1973; Vol. I, p 154.
(9) Randall, J. C. *Polymer ACS Symp. Ser.* **1980**, *No. 142*, 94-118.
(10) Elsner, G.; Riekel, C.; Zachmann, H. G. *Polymer Science*; Springer-Verlag: New York, 1985; Vol. 67, pp 1-57.
(11) Riekel, C.; Heuer, J.; Lux, H.; Zachmann, H. G.; Zietz, R. *Jahresber. Hasylab* **1985**, 267.
(12) Boulin, C.; Dainton, D.; Dorrington, E.; Elsner, G.; Gabriel, A.; Bordas, J.; Koch, M. H. J. *Nucl. Instrum. Methods Phys. Res.* **1982**, *201*, 209.
(13) Fischer, E. W.; Kloos, F.; Lieser, G. *J. Polym. Sci., Polym. Lett. Ed.* **1969**, *7*, 845.
(14) Van Krevelen, D. W. *Properties of Polymers*; Elsevier: Amsterdam, 1976.
(15) Swan, P. R. *J. Polym. Sci.* **1960**, *42*, 525.
(16) Schouterden, P. Ph.D. Thesis, Leuven, 1988.
(17) Strobl, G. R.; Schneider, M. J.; Voight-Martin, I. G. *J. Polym. Sci., Polym. Phys. Ed.* **1980**, *18*, 1361.
(18) Fischer, E. W.; Martin, G.; Schmidt, G. F.; Strobl, G. *Proc. IUPAC Symp.* **1968**.
(19) Schultz, J. M.; Fischer, E. W.; Schaumburg, O.; Zachmann, H. G. *J. Polym. Sci., Polym. Phys. Ed.* **1980**, *18*, 239.
(20) Norton, D. R.; Keller, A. *J. Mater. Sci.* **1984**, *19*, 447.
(21) Dlugosz, J.; Fraser, G. V.; Grubb, D.; Keller, A.; Odell, J. A.; Goggin, P. L. *Polymer* **1976**, *17*, 471.
(22) Vonk, C. G.; Kortleve, G. *Kolloid Z.Z. Polym.* **1967**, *220*, 19.
(23) Vonk, C. G.; Pijpers, A. P. *J. Polym. Sci., Polym. Phys. Ed.* **1985**, *23*, 2517.
(24) Schouterden, P.; et al., to be submitted for publication.
(25) Holdsworth, P. J.; Keller, A. *J. Polym. Sci., Polym. Lett. Ed.* **1967**, *5*, 605.
(26) Martinez Salazar, J.; Baltá Calleja, F. J. *J. Cryst. Growth* **1980**, *48*, 283.
(27) Cagiao, M. E.; Baltá Calleja, F. J. *J. Macromol. Sci., Phys.* **1982**, *B21*(4), 519.
(28) France, C.; Hendra, P. J.; Maddams, W. F.; Willis, A. *Polymer*, **1987**, *28*, 710.
(29) Lauprêtre, F.; Monnerie, L.; Barthelemy, L.f Vairon, J. P.; Sauzeau, A.; Roussel, D. *Polym. Bull. (Berlin)* **1986**, *15*, 159.

Horizontally Oriented Microdomains of Block Copolymers by Means of Segment–Segment Interactions

Koji Ishizu* and Takeshi Fukuyama

Department of Polymer Science, Tokyo Institute of Technology 2-12, Ookayama, Meguro-ku, Tokyo 152, Japan. *Received February 24, 1988; Revised Manuscript Received June 16, 1988*

ABSTRACT: Well-defined poly(styrene-*block*-isoprene) diblock copolymers were prepared by sequential anionic addition. Composite films were fabricated by casting these block copolymer solutions on a surface of cross-linked polystyrene as a substrate film and by varying the casting solvent. The control of horizontally oriented microdomains of block copolymers is discussed in terms of the morphology of the composite films.

Introduction

Block copolymers composed of incompatible block segments generally form a microdomain structure in the solid state as a consequence of microphase separation of the constituent block chains. The morphology of diene-containing block copolymers has been most extensively studied and found to depend, according to Molau's rule,[1] on the conditions of preparation, for example, the type of casting solvent.[1-3] These studies have been concerned with the morphology of the microdomain in solids. O'Malley et al.[4] have investigated the surface properties of block copolymers and, in particular, their surface composition and topography at the air–copolymer interface. They have made clear that the surface and bulk were not identical because of the significant differences in the solid-state surface tension of each block. More recently, Hasegawa et al.[5] have studied the morphology of the microdomains of an AB diblock copolymer formed as a consequence of liquid–liquid microphase separation of the constituent polymer A and B at or near the air–polymer interface in constrast to the morphology in the bulk. It was found that the morphology at the surface was dramatically affected by the surface free energy. In preceding papers,[6-9] we have established a preparation method for vertically oriented microdomains of block and graft copolymers or polymer blends by means of an epitaxial growth of a microdomain pattern on the surface of the substrate film.

In this paper, well-defined poly(styrene (S)-*block*-isoprene (I)) diblock copolymers were prepared by sequential anionic addition. The aim of this work is to describe the control of the microdomain structure (horizontally oriented lamellar and cylindrical microdomains) of poly(S-*b*-I) diblock copolymers by means of the segment–segment interactions between one component of diblock copolymer and substrate film.

Experimental Section

Polymer Synthesis. Poly(S-*b*-I) diblock copolymers were prepared by living anionic polymerization techniques. Styrene was first dried over a mixture of calcium hydride–lithium aluminum hydride and then purified with triphenylmethylsodium in vacuum. Isoprene was dried over calcium hydride and then purified with *n*-butyllithium (*n*-BuLi) in vacuum. Benzene was

0024-9297/89/2222-0244$01.50/0